High Aspect Ratio Conjugated Polymer Nanowires for High Performance Field-Effect Transistors and Phototransistors

Hyun Ah Um,[†] Dae Hee Lee,[†] Dong Uk Heo,[†] Da Seul Yang,[†] Jicheol Shin,[†] Hionsuck Baik,*[,‡] Min Ju Cho,*[,†] and Dong Hoon Choi*[,†]

[†]Department of Chemistry, Research Institute for Natural Sciences, Korea University 5 Anam-dong, Sungbuk-gu, Seoul 136-701, Republic of Korea and [‡]Division of Analytical Research, Korea Basic Science Institute, 74 Inchon-ro, Sungbuk-gu, Seoul 136-713, Republic of Korea

ABSTRACT We synthesized a highly crystalline DPP-based polymer, DPPBTSPE, which contained 1,2-bis(5-(thiophen-2-yl)selenophen-2-yl)ethene as a planar and rigid electron donating group. High- and low-molecular weight (MW) DPPBTSPE fractions were collected by Soxhlet extraction and were employed to investigate their unique charge transport properties in macroscopic films and single crystalline polymer nanowire (SC-PNW), respectively. The low-MW polymer could provide well-isolated and high aspect ratio SC-PNWs, in which the direction of $\pi-\pi$ stacking was perpendicular to the wire growing axis. The field effect transistors made of SC-PNWs exhibited remarkably high carrier mobility of 24 $cm^2 V^{-1} s^{-1}$. In addition, phototransistors (PTs) made of SC-PNW showed very high performance in terms of photoresponsivity (R) and photoswitching ratio (P). The average R of the SC PNW-based PTs were in the range of 160–170 A W^{-1} and the maximum R was measured at 1920 A W^{-1}, which is almost three orders higher than that of thin film-based PT device.

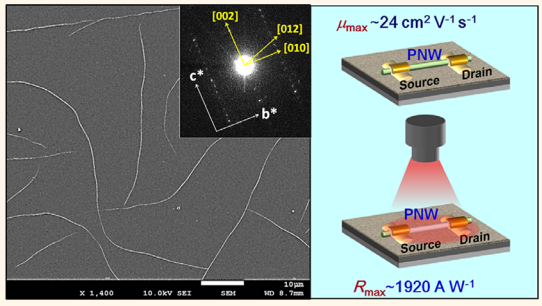

KEYWORDS: diketopyrrolopyrrole · selenophene · polymer nanowire · field-effect transistor · phototransistor

Past research on organic semiconductors predominantly focused on *p*-type small molecules such as the polyacene, fused thiophene, and thienoacene derivatives. Field effect transistors (FETs) using these organic semiconductors demonstrated carrier mobility as superb as 20–40 $cm^2 V^{-1} s^{-1}$, thereby earning these semiconductors a reputation as materials that could replace inorganic semiconductors.[1] It was further observed that single-crystal and polycrystalline devices using organic semiconductors' microplates, micro/nanowires, nanofibers, nanoribbons, *etc.*, exhibited superior carrier mobility compared to that of the thin film-based FETs.[2−10] In addition to outstanding charge transport behavior, photoinduced charge generation of organic semiconductors also have great attention in promising optoelectronic devices such as phototransistors (PTs) owing to their high photosensitivity and photoinduced modulation of electrical property.[10−12]

Until recently, the charge transport properties of semiconducting polymers have generally been recognized as inferior to those of semiconducting small molecules because of their chain disorder in the solid state. However, certain polymers are increasingly drawing attention for their high performance in field-effect transistors (FETs),[13−15] phototransistors (PTs)[16,17] and photovoltaic devices.[18,19]

Further, rapid progress has been achieved in the development of high performance semiconducting polymers with highly extended π-conjugation systems, and highly crystalline polymers have come to be accepted as suitable materials for the active channels in large-scale thin-film transistor (TFT) devices.[20−22] In particular, the use of the donor–acceptor (D–A) concept to create an alternating semiconducting copolymer structure has been demonstrated as a highly efficient strategy for improving semiconductor performance. In these structures, conjugated electron-donor and acceptor units are employed to reduce the bandgap energies[23] and the $\pi-\pi$ stacking distance between polymer chains (<3.8 Å).[24,25] Because of these properties, D–A polymers

* Address correspondence to baikhs@kbsi.re.kr, chominju@korea.ac.kr, dhchoi8803@korea.ac.kr.

Received for review January 30, 2015 and accepted May 11, 2015.

Published online May 11, 2015
10.1021/acsnano.5b01982

exhibit superior charge-carrier mobility as compared to conjugated polymers bearing only donor moieties.[26−28]

Especially, among D−A polymers, diketopyrrolopyrrole (DPP)-based conjugated polymers are regarded as highly promising materials for achieving future high-performance organic FETs.[29−31] Since DPP unit has a intrinsically strong symmetric acceptor with a fused ring structure, corresponding polymers could boost up the crystallinity and semiconducting property by introducing various symmetric and rigid donating groups. Although a number of studies have demonstrated the outstanding characteristics of D−A polymers, not many precise studies have been conducted to investigate the charge-transport and photoinduced charge generation properties of nanoscopic objects of these polymers.

In the case of conjugated small molecules, the charge-transport and photoinduced charge generation properties are often investigated using single-crystalline (SC) objects.[32,33] Among various types of nanoscopic objects, single-crystalline nanowires (NWs) were often employed to study their intrinsic electronic and optoelectronic properties.[34−37] In the case of conjugated polymers with D−A repeating units featuring long polymer chains, chain disorders, and various undesirable impurities, it is difficult to grow single-crystalline structures and study their charge-transport properties on the micro- and nanoscopic scales. Therefore, the charge-transport properties of polymer films can be partially predicted through atomic force microscopy (AFM) and grazing incidence X-ray diffraction (GI-XRD) measurements. Many scientists have recognized the importance of the orientation and packing of the polymer chains in the solid state, but few have investigated these properties and the resulting electronic properties using NWs[34−37] and nanofibers.

Despite the low volume of published research work, specialized research on and attempts at fabrication of polymer semiconductors in general continued. This effort has produced crystalline polymer micro/nanowires using specific semicrystalline conjugated polymers fabricated through solvent vapor annealing method.[38−40] The devices with 1D single-crystalline polymer micro/nanowires were observed to significantly enhance the dark and photoinduced charge transport properties in FET devices, owing to their long-range-order of polymer chains. This attempt ushered in the great possibility that D−A type conjugated copolymers could be used to fabricate high performance FETs and related devices with charge transport channels that employ single or multiple NWs.

In our previous work, we had demonstrated that SC polymer NWs (SC-PNWs) could be fabricated from a DPP-based copolymer, PDTTDPP bearing dithienothiophene (DTT) in the repeating group.[34] However, this polymer showed a relatively poor ability to form NWs, which were limited to short lengths. Furthermore, the corresponding SC-PNW FET exhibited a lower charge carrier mobility than we expected. These phenomena could have resulted from the large polydispersity index (PDI = 7.0) of the polymer and from the particular arrangement of the DTT donating unit in the repeating group in the SC structure, which could interfere with the longitudinal growth of the NWs. Therefore, it might be useful to control the molecular weight (MW) or the PDI of DPP-based polymers and to introduce a properly designed donating unit in the polymer backbone to allow for the longitudinal growth of NWs of the polymer.

In this study, a highly crystalline DPP-based polymer (DPPBTSPE) bearing 1,2-bis(5-(thiophen-2-yl)-selenophen-2-yl)ethene in the repeating group was synthesized (Supporting Information Scheme 1S). Molecular weight fractionation of the synthesized polymer was carried out to yield high- and low-MW DPPBTSPE by Soxhlet extraction. Two fractions were employed to investigate their unique charge transport properties in macroscopic films and SC-PNW. Because the low MW polymer is capable of forming well-isolated single-crystalline PNW, it was employed to prepare the SC-PNW-based FETs; the SC-PNWs exhibited unprecedentedly high carrier mobility over 20 $cm^2 V^{-1} s^{-1}$, since intramolecular charge transport was facilitated along the growth direction of the NWs. In addition, a low-MW DPPBTSPE-based PNW phototransistor (PT) showed relatively much higher photoresponsivity than thin-film-based PT devices

RESULTS AND DISCUSSION

In our previous communication, we have demonstrated P(DPP-*alt*-DTBSe) as one of the promising selenophene-containing polymers. It performed a higher carrier mobility (μ = 1.50 $cm^2 V^{-1} s^{-1}$) and other better device parameters than that of the previous reported bithiophene containing DPP-polymer did.[20,41] It is attributed to strong electron donating property of selenophene and the formation of more favorable quinoidal structures of biselenophene derivatives. Therefore, we became interested in altering the structure of the above polymer to enhance the semiconductor performance and thus came to design a similar polymer. Herein, we synthesized a similar polymer, DPPBTSPE, by introducing 1,2-bis(5-(thiophen-2-yl)-selenophen-2-yl)ethene (BTSPE) into the repeating group (Scheme 1S). In a geometrical aspect, the repeating groups of DPPBTSPE lined up along the direction of the polymer chain, in contrast to the repeating groups of PDTTDPP (Figure 1a and Figure 1S).[34] In addition, the electron-donating moiety, selenophene, in the polymer induces a well-ordered polymer chain arrangement on the substrate, due to its strong intermolecular interactions.[20,29]

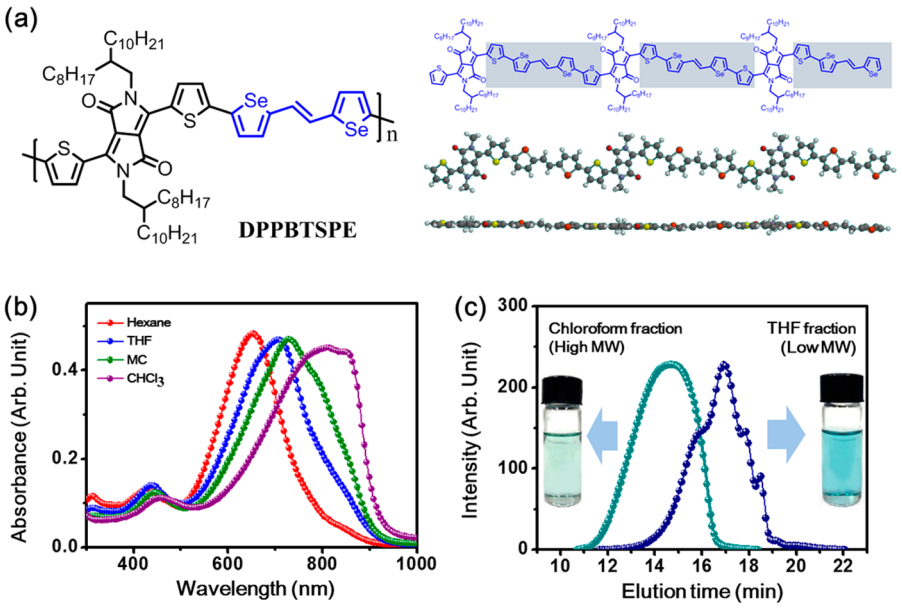

Figure 1. (a) Molecular structure of DPPBTSPE. Schematic illustration of three repeating groups along the polymer chain and optimized geometry of trimer. (b) UV−vis absorption spectra of polymer solutions collected during Soxhlet extraction. (c) GPC curves of DPPBTSPE obtained from the THF and chloroform fractions. Insets: Solutions of high-MW (left) and low-MW (right) DPPBTSPE.

After synthesizing the polymer DPPBTSPE *via* Stille coupling reaction, we fractionated it by Soxhlet extraction using various solvents. The UV−vis absorption spectra of the four solvent fractions of DPPBTSPE are shown in Figure 1b. The absorption maxima (λ_{max}) of the solutions of the hexane, tetrahydrofuran (THF), methylene chloride (MC), and chloroform fractions were 620, 708, 730, and 850 nm, respectively. This spectral comparison demonstrates that the absorption band attributable to intramolecular charge transfer along the polymer chain shifted sequentially to longer wavelengths from the hexane fraction to the chloroform fraction. It is conjectured that this large bathochromic shift is due to an increase in the MW of the fractionated polymeric species.[42−44]

Of these four fractions, we collected the largest amount of the polymer products in the THF and chloroform fractions; these were then used for further characterization and device fabrication. The MWs of DPPBTSPE in these two fractions were determined using gel permeation chromatography (GPC), which was performed at 35 °C using chloroform as the eluent. The number-average MW (M_n) values of the THF and chloroform fractions were determined to be 8 kDa (low-MW) and 68 kDa (high-MW), respectively, and their PDI values were determined to be 2.57 and 2.10, respectively (Figure 1c). With respect to the two insets in Figure 1c, the color of the dilute solution bearing the high-MW polymer is light green, whereas the color of the low-MW polymer solution is pale blue. This is because of the difference in the absorption behaviors of the two polymer fractions in the visible and near-infrared (IR) region as well as in their bandgap energies.

It can be seen from Figure 2a−f that PNWs of DPPBTSPE could be fabricated successfully; the aspect ratio of the PNWs was controlled using the two polymer fractions. Using the two polymer samples with different MWs, we prepared dilute solutions (concentration of 0.001 wt %) in MC as the solvent (low-MW) and in chloroform/MC as the solvent (1:4 v/v, high-MW). Low-MW DPPBTSPE is slightly soluble in methylene chloride (MC) and the polymer chains are apt to undergo self-association for generate nuclei in solution state. In the case of high-MW DPPBTSPE, good solubility in chloroform and very poor solubility in MC were observed. Therefore, for nucleation process, we added small amount of chloroform into MC (MC/chloroform = 4:1) and prepared *marginal* solvent mixture for nucleation and growth of NWs. These solutions were then stored for 72 h under ambient conditions. When the low-MW DPPBTSE was dissolved in MC as a marginal solvent, some nuclei were generated by assembling a few polymer chains. Then, it was found that primary assemblies of polymer chains were formed through the growth of nuclei. The corresponding primary assemblies congregated to give larger assemblies of polymer chains resulting in the formation of premature polymer nanowire. Eventually, the long polymer nanowires could be generated through fusion of the nanoscopic assemblies.[45,46]

Figure 2a,b shows optical microscopy (OM) images of the PNWs made from the high- and low-MW polymers, respectively; the PNWs were fabricated on *n*-octyltrichlorosilane (OTS)-SiO_2/Si substrates. Figure 2c,d contains scanning electron microscopy (SEM) images showing the sizes and shapes of the individual PNWs.

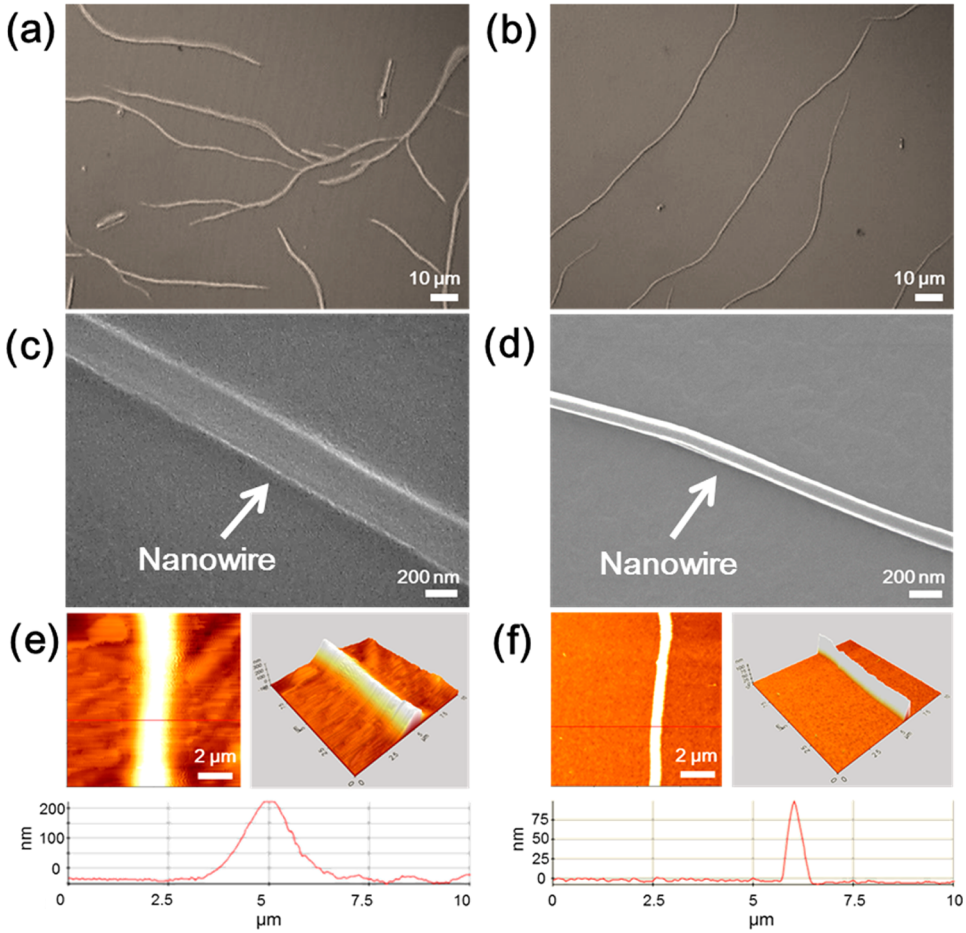

Figure 2. (a and b) OM images of NWs of (a) high- and (b) low-MW DPPBTSPE. (c and d) SEM images of single NWs of (c) high- and (d) low-MW DPPBTSPE. (e and f) 2D and 3D AFM height images of single NWs of (e) high- and (f) low-MW DPPBTSPE. The surface profiles are also included.

It can be seen that the PNW grown from the solution of the high-MW polymer is significantly wider than that grown from the low-MW polymer obtained from the THF fraction (length > 50 μm, width $\approx$ 170 nm). Interestingly, the length of the PNW of the low-MW polymer was greater than 100 μm and much longer than that of the PNW made of the high-MW polymer. In brief, the aspect ratio (300−600) of the PNW made of low-MW polymer is much larger than that of the PNW made of high-MW polymer. (Figure 4S)

To investigate the PNWs in detail, we obtained AFM images of the PNWs; these are shown in Figures 2e,f. The two AFM images appear drastically different, even though they are at the same magnification level. Figure 2e shows a rough landscape with a thick ridge bulging among a number of protuberances. Upon careful inspection, less-pronounced ridges can be observed submerged under the layers of lithosphere and crust. Figure 2f features a sharper ridge, which projects above a flat surface in the absence of other visible protuberances. From these results, it can be surmised that NWs of DPPBTSPE can be formed from dilute solutions. However, the internal morphology of these NWs cannot be investigated using OM, SEM, or AFM.

Figure 3 shows transmission electron microscopy (TEM) images of the PNWs of the high- and low-MW DPPBTSPE fractions and the corresponding selected-area diffraction (SAED) patterns. Although the PNWs of the high-MW polymer could be observed in the SEM and AFM images, the TEM images showed an intriguing feature in that the PNWs were caged within a network structure. At first glance, the image in Figure 3a appears to be a fractal, but in fact, it has no geometric pattern except for the existence of single NW. The random crystalline domains appear to be layered and interwoven in no particular arrangement; this was confirmed further from the SAED pattern (*i.e.*, ring pattern) in Figure 5Sc, and they are in fact touching each other as if connected.

The image in Figure 3b, on the other hand, does not show the large-area random crystalline domains but instead shows small dark spots of various sizes (*i.e.*, length <10−20 nm) and shapes, which are scattered in no particular pattern; the corresponding SAED image, shown in Figure 6Sc, has no obvious diffraction pattern. Therefore, the NWs of the low-MW polymer could be isolated and used to fabricate single-wire-based devices. The two kinds of PNWs exhibited almost identical

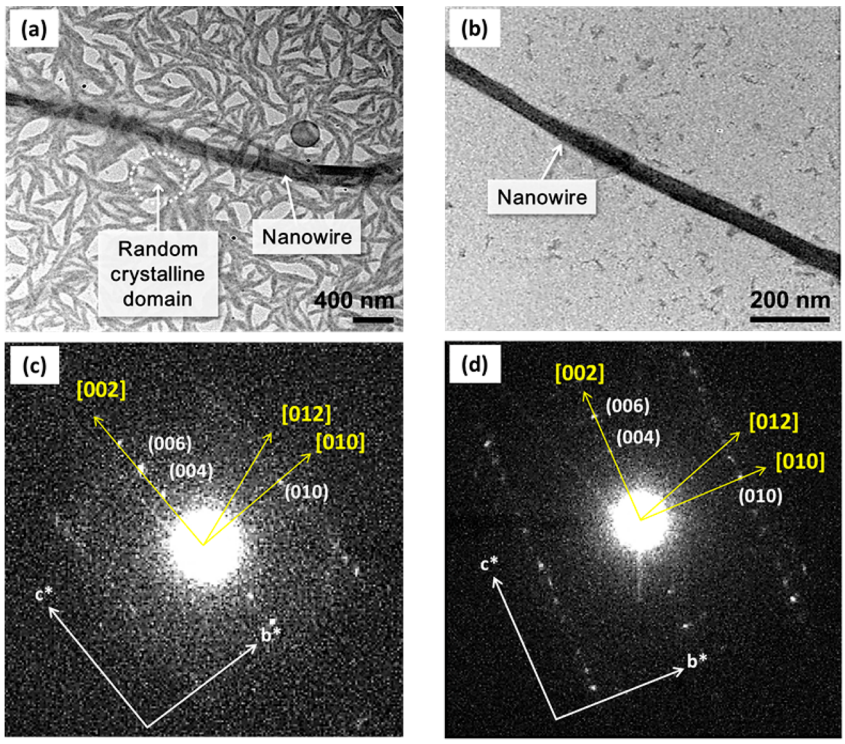

Figure 3. (a and b) TEM images of PNWs made of (a) high- and (b) low-MW DPPBTSPE. (c and d) SAED patterns of PNWs made of (c) high- and (d) low-MW DPPBTSPE. The patterns were taken perpendicular to the long axis of the PNW.

diffraction behaviors that confirmed their SC character, even though slight scattering could be observed (see Figure 3c), owing to the presence of random crystalline domains that overlapped with the PNWs. Furthermore, the polymer chains confined in the NW were aligned parallel to the long axis of the PNW, as is obviously supported by the observation of (004), (006), and (010) diffraction patterns. It is notable that the PNWs did exhibit similar diffraction patterns when the electron beam was moved along the NW and it did not vary from NW to NW, indicating that the fabricated PNWs were single crystals (Figure 8S).

In addition to the SAED analysis of the PNWs, GI-XRD analysis was performed too, to determine their two-dimensional (2D) diffraction patterns. These patterns were obtained using PNWs fabricated on OTS-SiO_2/Si substrates and supported the above-mentioned results. The sample used for the GI-XRD analysis appeared to consist of numerous randomly orientated nanowires and a few small pieces of polymer film.

As can be seen in Figure 4, the 2D XRD pattern of the sample was completely different from that of thermally annealed thin film of the polymer and consisted of ring patterns, indicating polycrystallinity. We observed distinct ring patterns close to the center; these could be assigned to the (*h*00) diffractions (Figure 4b). Since a (200) diffraction peak was clearly observed, the (100) spacing ($d_{(100)}$ = 18.98 Å) could be calculated accurately.

To support this observation, we have plotted the in-plane diffraction profile of the PNWs in Figure 4d. Two sharp diffraction peaks could be observed at 3.19° and 18.54°; these were markedly different from those in the in-plane profile of the thermally annealed film shown in Figure 4c. Further, the fact that the widths of the two diffraction peaks were very small implies that the peaks arose owing to the SC nature of the PNWs. In this in-plane profile, the $d_{(010)}$-spacing was accurately determined to be 3.46 Å, which indicates $\pi-\pi$ stacking distance in the PNW. Combining the results of SAED and GI-XRD, we could calculate $d_{(001)}$-spacing of 20.34 Å.

From the SAED and GI-XRD patterns of the PNWs, it was determined that the SC PNWs had an orthorhombic unit cell whose lattice constants were $a \approx 18.98$ Å, $b \approx 3.46$ Å, and $c \approx 20.34$ Å ($\alpha = \beta = \gamma = 90°$). Thus, the "*b*" value, owing to the $d_{(010)}$ spacing of the PNWs was much smaller than that of the polymer thin film ($d_{(010)}$ = 3.72 Å in Figure 4c), which indicated that the polymer chains were packed more densely in the SC-PNWs and occupied the lowest possible volume in the unit lattice. The arrangement of the polymer chains within the SC-PNWs is depicted in Figure 4e. A possible configuration of the orthorhombic lattice unit cell was defined on the basis of the results of the GI-XRD and TEM analysis. From the structure analysis, it was concluded that the DPPBTSPE chains in the SC-PNWs were lined up unidirectionally and parallel to the long axis of the NWs. While polymer microwires and PNWs with a SC structure have been reported previously,[36] this is the first time that high aspect ratio SC-PNWs of a DPP-based polymer bearing a selenophene donor moiety

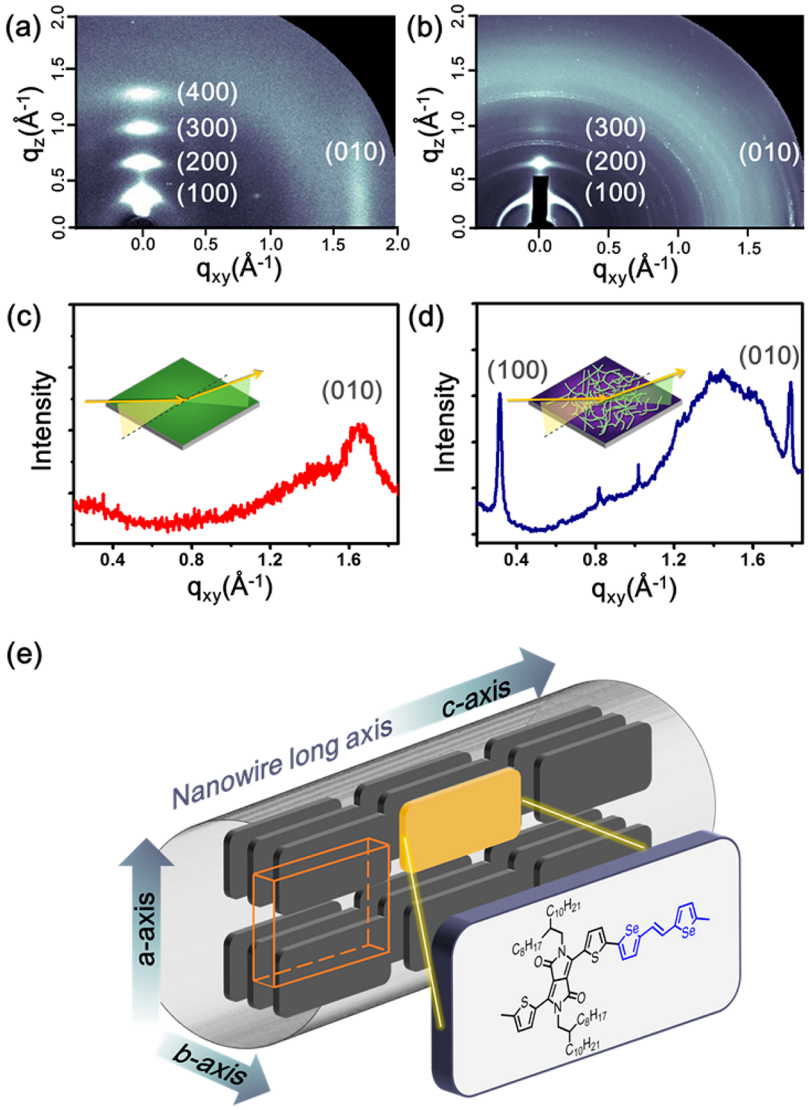

Figure 4. (a) 2D XRD pattern of a thermally annealed film of low-MW DPPBTSPE deposited on OTS-SiO_2/Si substrate. (b) 2D XRD pattern of PNWs deposited on OTS-SiO_2/Si substrate. (c) 1D in-plane profile of thermally annealed polymer film. (d) 1D in-plane profile of PNWs of low-MW DPPBTSPE. (e) Schematic diagram of the orientation of polymer chains and the possible orthorhombic crystal unit cell in the SC-PNWs.

and having a relatively long repeating group have been fabricated and the lattice parameters in the SC have been determined from the SAED and 2D XRD patterns of the PNWs.

Next, to compare the macroscopic charge transport properties of polymer samples with these two different MWs, low- and high-MW-polymer-based TFTs were fabricated. All the evaluated TFT devices displayed *p*-type semiconducting behavior under ambient conditions. The maximum hole mobilities of the pristine films of low- and high-MW DPPBTSPE were measured to be 1.06 and 1.53 $cm^2\ V^{-1}\ s^{-1}$. After subsequent thermal annealing, the mobility values increased to 2.10 and 4.15 $cm^2\ V^{-1}\ s^{-1}$, and a reasonably high on−off current ratio of $>10^6$ was maintained (Figures 9S and 10S). As is well-known, the higher mobilities were attributed to the fact that thermally annealed films of the low and high MW polymers showed a prominent edge-on orientation in accordance with the high intensity (010) diffraction peak and the disappearance of the (100) diffraction peak in the in-plane profiles (Figure 11S).

It was also found that the high-MW polymer exhibited much better charge transport properties than the low-MW polymer because of the uniformly intertwined nanofibers and densely packed chain networks in the thin film, as shown in Figure 12Sb,d. This structure could facilitate efficient charge transport behaviors by minimizing the barrier between crystalline domains.[47]

Of the two MW polymer samples, low-MW DPPBTSPE yielded well-isolated and high aspect ratio PNWs, which were used to investigate its charge-transport properties. In the case of high-MW DPPBTSPE, the PNWs were embedded in a multilayered interwoven random crystalline network, which made it difficult to fabricate FET devices for observing the charge-transport property

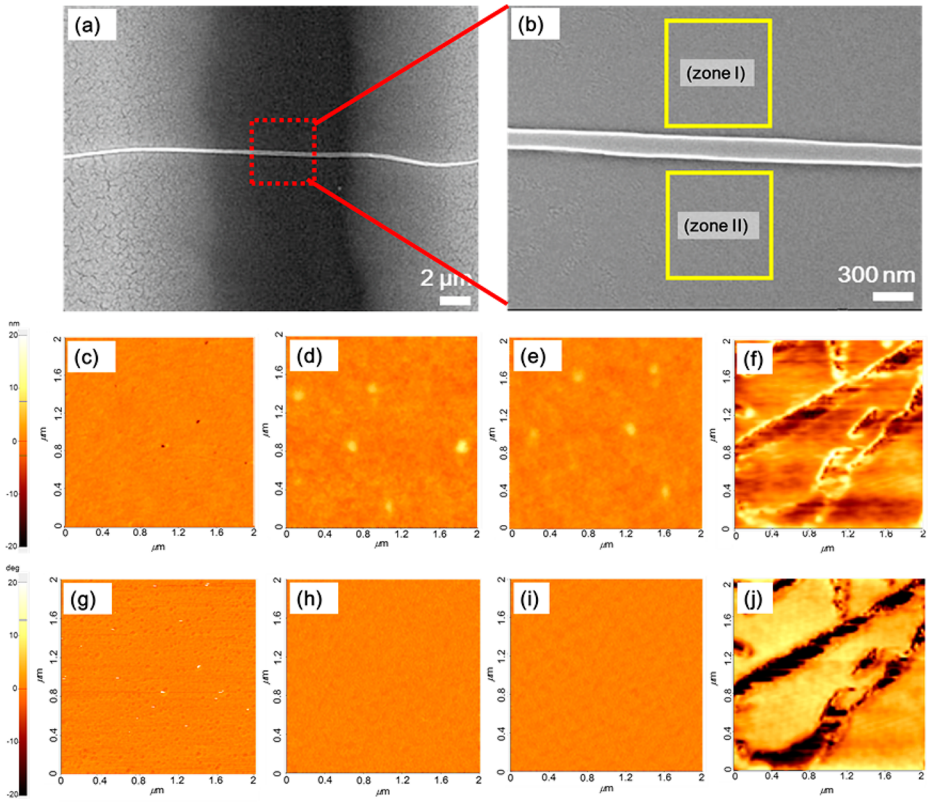

Figure 5. (a and b) SEM images of the SC PNW-based FET. (c and g) OTS-SiO_2/Si. (d and h) zone I; (e and i) zone II; (f and j) film prepared by spin-coating the solution of the polymer in MC. (c–f) Height images; (g–j) phase images.

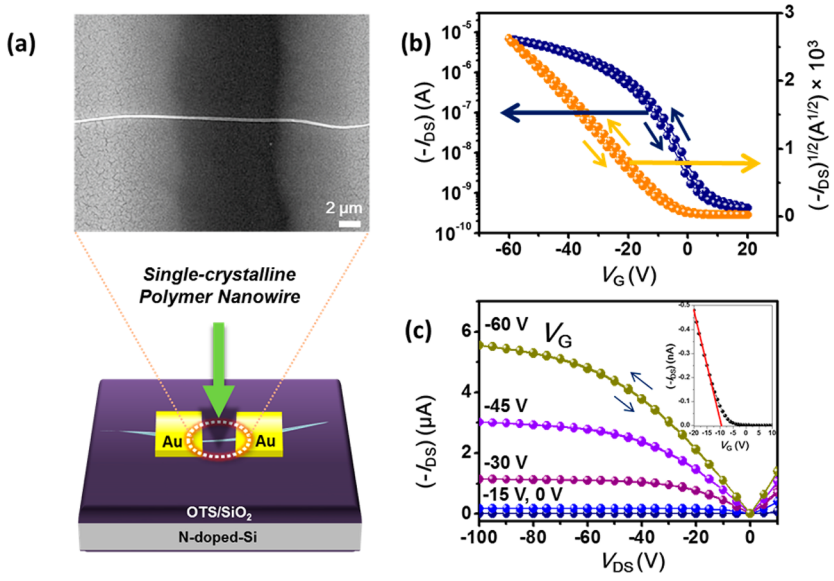

Figure 6. (a) SEM image of a FET device based on a SC-PNW of low-MW DPPBTSPE and schematic diagram showing the device configuration. (b and c) Transfer and output curves of the SC-PNW FET device (V_{DS} = −60 V, linear V_G range; −5 to −60 V). Inset: Transfer characteristics in the linear regime of the SC-PNW FET device (V_{DS} = −5 V).

of an individual PNW (Figure 3a). On the other hand, a PNW of low-MW DPPBTSPE could be isolated and was long enough (length of 50–100 μm) to facilitate the deposition of gold electrodes with a long channel (channel length of ~10 μm).

The representative SEM image of the device, shown in Figures 5a and 6a, shows a single NW between two gold electrodes; the NW width is 170 nm and the channel length is 10.62 μm. The SEM image confirms the well-defined structure of an isolated PNW, indicating that it could be used for device characterization.

Although no large pieces or patches of the polymer film were observed in Figure 3b, AFM (2 μm × 2 μm) was employed to observe the area adjacent to the PNW

TABLE 1. Device Parameters of the TFTs and the SC-PNW-Based FET

polymer	M_n (kDa)	device	W/L (μm/μm)	$T_{annealing}$ (°C)	μ_{sat} (cm^2 V^{-1} s^{-1})	I_{on}/I_{off}	V_{th} (V)
Chloroform fraction	68	TFT	1500/100	Pristine	2.10	10^8	0
				250	4.15	10^8	0
THF fraction	8	TFT	1500/100	Pristine	1.06	10^8	−7
				200	1.53	10^6	6
		PNW-FET	0.17/10.62	Pristine	24.0[a]	10^4	−4

[a] Maximum mobility.

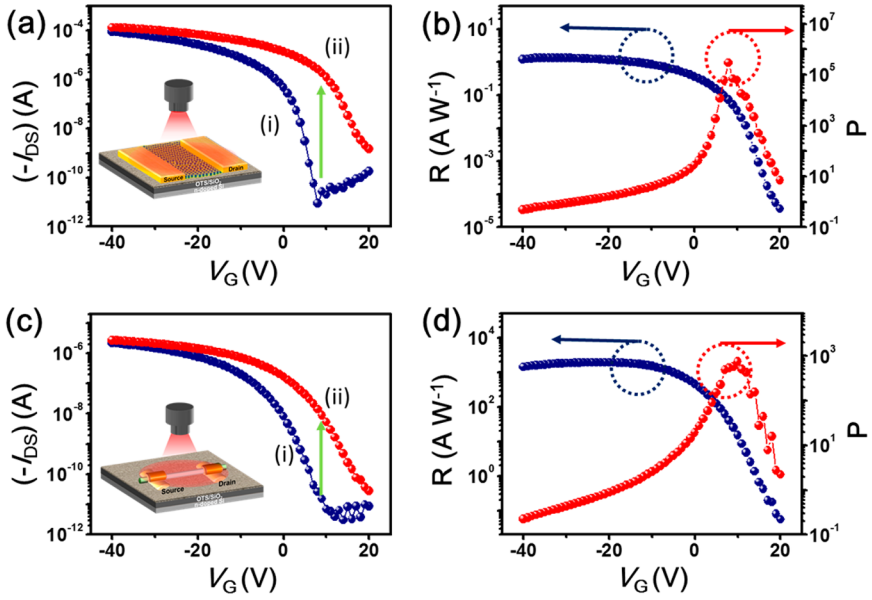

Figure 7. (a and c) Transfer curves of OPTs in the dark (i) and under monochromatic light irradiation (ii) (λ = 632 nm, I = 24 mW cm^{-2}). (b) Photoresponsivity (R) and photoswitching ratio (P) *vs* V_G for the TFT. V_{DS}= −40 V; (d) R and P *vs* V_G for the SC PNW FET, V_{DS}= −30 V.

more precisely. The obtained height and phase images were compared to those of the surface of the OTS-SiO_2/Si substrate as well as those of the surface of a thin film of a MC solution (concentration of 1 mg mL^{-1}). As can be seen in Figure 5, the height and phase images of zones I (d and h) and II (e and i) were not very different from those of the OTS-SiO_2/Si substrate. In addition, the surface topography and phase image of the ultrathin film made from MC solution (*i.e.*, thickness of <8 nm) was markedly different from those of zones I and II. Therefore, even though a few tiny polymer particles were present around the PNW of low-MW DPPBTSPE, no detrimental film channel was observed between the two electrodes. This confirmed that the output and transfer curves displayed herein were based only on the current flowing through the single PNW.

By characterizing more than 20 SC-PNW FET devices, the carrier mobilities could be determined and were found to be 15−24 cm^2 V^{-1} s^{-1}. Further, the current on/off ratio was found to be 10^4. The large variation might be attributed to the poor interfacial contact of PNW on gate insulator, physical defect along the nanowire, or crumpled surface of nanowire.[48,49]

For instance, the highest carrier mobility of 24.0 cm^2 V^{-1} s^{-1} was calculated with the linear slope between −5 and −60 V (Figure 6b and Table 1). Fairly low hysteresis was observed in the transfer curve over the entire range of applied gate voltages, because of the significantly low density of charge-trapping impurities or defects in this particular SC-PNW as well as at the interface between the PNW and the OTS-SiO_2/Si layer.[50,51] The unprecedentedly high carrier mobility of the FETs fabricated using the low-MW DPPBTSPE-based PNWs might be attributable to the uniform orientation of the polymer chain along the growth direction of the wire. This would lead to fast intramolecular charge transport along the PNW preferentially accompanied by less pronounced charge-carrier hopping.[35]

Besides excellent charge transport properties, photoinduced exciton generation and its contribution to the performance of PT devices have been investigated. The PT performances were investigated by using the low-MW DPPBTSPE-based TFT and PNW-based FET devices which were already used in this study. In the PT devices, enhancement of the drain current (I_{DS}) was demonstrated under light illumination (λ = 632 nm,

I = 24 mW cm^{-2}). First, it was found that the large increase in I_{DS} was induced by illumination of light ($I_{DS}^{photo}/I_{DS}^{dark} \sim 10^3-10^4$) and that the threshold voltage was significantly shifted to a positive gate bias, which was attributed to photodoping.[52,53] (Figure 7a,c) For the electrons induced by photoexcitation, they could be trapped at the interface between PNW and gate insulator. The trapped electrons acted like a negative gate voltages and they induced accumulation of additional holes in the single PNW, resulting in a large increment of I_{DS}. The detailed mechanism of phototransistor behavior was well explained in the previous literatures.[32,33,54]

From two transfer curves in Figure 7a,c, two important parameters such as photoresponsivity (R) and photoswitching ratio (P) could be determined. In Figure 7b,d, R and P are plotted *versus* V_G for the film- and PNW-based PT devices made from low-MW DPPBTSPE. For instance, the P and R values of the PNW-based PT device were determined at around the crossing point of the two curves with V_{DS} = +4.0 V. The average R of the SC PNW-based PTs were in the range of 160−170 A W^{-1}; $R_{max} \sim$ 1920 A W^{-1}, which is almost three orders higher than that of thin film-based PT device. It is mainly attributed to highly ordered polymer chain packing and very efficient exciton dissociation in a SC-PNW without possible charge carrier recombination.

To the best of our knowledge, there was no report on phototransistor behavior in the SC PNWs devices made of selenophene-DPP based conjugated polymer. The R and P in this study are the markedly high values for low-MW DPPBTSPE-based PNW PTs without thermal annealing due to densely packed polymer chains in NWs and very efficient inter/intramolecular exciton generation and dissociation in SC PNWs.

CONCLUSIONS

We prepared the conjugated copolymer DPPBTSPE bearing DPP and BTSPE units into two fractions with low- and high-MW. SC-PNWs were successfully fabricated by solution processing. The low-MW polymer formed well-isolated SC-PNWs with relatively higher aspect ratio, in which the direction of $\pi-\pi$ stacking was perpendicular to the direction of the long axis of the PNWs. FET devices fabricated from individual SC-PNWs of low-MW DPPBTSPE exhibited a maximum hole mobility of 24.0 cm^2 V^{-1} s^{-1}. The mobility in the linear region was also measured and found to be approximately 4.78 cm^2 V^{-1} s^{-1} at V_{DS} = −5 V. This saturated mobility was more than 20 times higher than that of a TFT device based on a thin film of the same polymer and can probably be improved further by optimizing the device configuration. In addition to remarkable charge-transport behavior, very intriguing photoinduced exciton generation and dissociated charge transport could be investigated in phototransistors (PTs) elaborated with SC-PNW. A PNW-based PT showed very high performance in terms of photoresponsivity and photoswitching ratio. The highly ordered single-crystalline selenophene-containing PNWs displayed much better electronic and optoelectronic device performance compared with thin-film-based corresponding devices.

METHODS

Polymer Nanowire Fabrication. The self-assembly method for preparing the polymer nanowires was as follows. DPPBTSPE was dissolved in methylene chloride (solvent for the low-MW fraction) and in chloroform/MC (1:4) (solvent for the high-MW fraction) in a concentration of 0.001 wt %. The solutions were heated to 35 °C for 10 min, resulting in complete dissolution of the solute, and then allowed to cool to room temperature. The vials containing the solutions were then capped and stored undisturbed at room temperature. After the solutions had been stored for 72 h under ambient conditions, they were drop-cast on the substrates at 90 °C to form well-defined SC-PNWs. The resulting NWs were heated on a hot plate for 15 min at 90 °C to remove the residual solvent.

Fabrication and Characterization of TFTs Made of DPPBTSPE. A bottom-gate top-contact device geometry was employed to evaluate the TFT performance of the two DPPBTSPE fractions. Spin-coated films of DPPBTSPE were deposited on heavily n-doped Si/SiO_2 substrates using chloroform as the solvent. To generate a hydrophobic dielectric surface, the silica surface was modified with OTS. Source and drain electrodes (80 nm) were then thermally deposited through a shadow mask; the width and length of the channel were 1500 and 100 μm, respectively. The saturated field-effect mobilities were measured in the saturation regime using the relationship: $\mu_{sat} = (2I_{DS}L)/(WC(V_G - V_{th})^2)$, where W is the channel width, L is the channel length, I_{DS} is the saturation drain current, C is the capacitance (∼11.5 nF cm^{-2}) of the dielectric SiO_2 (300 nm) per unit area, V_G is the gate bias, and V_{th} is the threshold voltage. The linear mobilities were calculated using the equation for the linear regime: $\mu = m_{linear}(L/W)(1/V_{DS})(1/C_i)$. The linear field-effect mobilities were calculated from the slope m_{linear} for low source-drain voltages; the slope was obtained from the plot of the source-drain current (I_{DS}) and the gate voltage (V_G). The device performances were evaluated under ambient conditions using a 4200-SCS semiconductor characterization system.

Fabrication and Characterization of PNW-Based FET/OPT Devices. NWs of low-MW DPPBTSPE were formed on OTS treated substrate with n-doped Si gate electrode and SiO_2 (300 nm) gate insulator. Subsequently, designed shadow masks were placed on individual low-MW PNWs. Next, 80 nm-thick source and drain Au electrodes were deposited on the PNWs by thermal evaporation using the shadow masks. The saturated field-effect mobilities of PNW-based FETs were measured in the saturation regime using the relationship: $\mu_{sat} = (2I_{DS}L)/(WC(V_G - V_{th})^2)$, where W is the width of PNW, L is the length of PNW, I_{DS} is the saturation drain current, C is the capacitance of the dielectric SiO_2 (300 nm) per unit area, V_G is the gate bias, and V_{th} is the threshold voltage. The FET device performance was measured in air using a 4200-SCS semiconductor characterization system. For the light source, a He−Ne laser with a neutral density filter was employed. The light illumination power was measured by using a Newport 2385-C Si photodetector with a calibration module. From the modulation of the transfer curve, we calculated the photoresponsivity (R) of the OPT device, defined as $\Delta I_{DS}/P_{inc}$, where ΔI_{DS} is $I_{DS}^{photo} - I_{DS}^{dark}$ and P_{inc} is the incident light intensity.

The photoswitching ratio (P) was obtained from ($I_{DS}^{photo} - I_{DS}^{dark}$)/$I_{DS}^{dark}$.

Conflict of Interest: The authors declare no competing financial interest.

Acknowledgment. This research was supported by National Research Foundation of Korea (NRF2012R1A2A1A01008797) and Basic Science Research Program through the National Research Foundation of Korea (NRF) funded by the Ministry of Education (NRF20100020209). We are grateful to Pohang Accelerator Laboratory (Pohang, Korea) for allowing us to conduct the grazing incidence X-ray diffraction (GI-XRD) measurements. We also thank KBSI for allowing the use of their HRTEM instrument.

Supporting Information Available: Detailed experimental procedure, molecular structures and geometry of trimer, thermal analysis data, cyclic voltammograms, SEM image, TEM/SAED images, transfer and output curves of TFTs made of low- and high-MW DPPBTSPE, and AFM images. The Supporting Information is available free of charge on the ACS Publications website at DOI: 10.1021/acsnano.5b01982.

REFERENCES AND NOTES

1. Klauk, H. Organic Thin-Film Transistors. *Chem. Soc. Rev.* **2010**, *39*, 2643–2666.
2. O'Carroll, D.; Iacopino, D.; Redmond, G. Luminescent Conjugated Polymer Nanowire Y-Junctions with On-Branch Molecular Anisotropy. *Adv. Mater.* **2009**, *21*, 1160–1165.
3. Richard-L, Marie.; Pellerin, C. Molecular Orientation in Electrospun Fibers: From Mats to Single Fibers. *Macromolecules* **2013**, *46*, 9473–9493.
4. Camposeo, A.; Greenfeld, I.; Tantussi, F.; Moffa, M.; Fuso, F.; Allegrini, M.; Zussman, E.; Pisignano, D. Conformational Evolution of Elongated Polymer Solutions Tailors the Polarization of Light-Emission from Organic Nanofibers. *Macromolecules* **2014**, *47*, 4704–4710.
5. Cai, Z.; Lei, J.; Liang, W.; Menon, V.; Martin, C. R. Molecular and Supermolecular Origins of Enhanced Electronic Conductivity in Template-Synthesized Polyheterocyclic Fibrils. 1. Supermolecular Effects. *Chem. Mater.* **1991**, *3*, 960–967.
6. Kakade, M. V.; Givens, S.; Gardner, K.; Lee, K. H.; Chase, D. B.; Rabolt, J. F. Electric Field Induced Orientation of Polymer Chains in Macroscopically Aligned Electrospun Polymer Nanofibers. *J. Am. Chem. Soc.* **2007**, *129*, 2777–2782.
7. Pagliara, S.; Vitiello, M. S.; Camposeo, A.; Polini, A.; Cingolani, R.; Scamarcio, G.; Pisignano, D. Optical Anisotropy in Single Light-Emitting Polymer Nanofibers. *J. Phys. Chem. C* **2011**, *115*, 20399–20405.
8. Persano, L.; Camposeo, A.; Pisignanoa, D. Active Polymer Nanofibers for Photonics, Electronics, Energy Generation and Micromechanics. *Prog. Polym. Sci.* **2015**, *43*, 48–95.
9. Wang, S.; Kappl, M.; Liebewirth, I.; Müller, M.; Kirchhoff, K.; Pisula, W.; Müllen, K. Organic Field-Effect Transistors based on Highly Ordered Single Polymer Fibers. *Adv. Mater.* **2012**, *24*, 417–420.
10. Guo, Y.; Du, C.; Yu, G.; Di, C.-a.; Jiang, S.; Xi, H.; Zheng, J.; Yan, S.; Yu, C.; Hu, W.; et al. High-Performance Phototransistors Based on Organic Microribbons Prepared by a Solution Self-Assembly Process. *Adv. Funct. Mater.* **2010**, *20*, 1019–1024.
11. Baeg, K.-J.; Binda, M.; Natali, D.; Caironi, M.; Noh, Y.-Y. Organic Light Detectors: Photodiodes and Phototransistors. *Adv. Mater.* **2013**, *25*, 4267–4295.
12. Guo, Y.; Xu, L.; Liu, H.; Li, Y.; Che, C.-M.; Li, Y. Self-Assembly of Functional Molecules into 1D Crystalline Nanostructures. *Adv. Mater.* **2015**, *27*, 985–1013.
13. Allard, S.; Forster, M.; Souharce, B.; Thiem, H.; Scherf, U. Organic Semiconductors for Solution-Processable Field-Effect Transistors (OFETs). *Angew. Chem., Int. Ed.* **2008**, *47*, 4070–4098.
14. Tsao, H. N.; Cho, D.; Andreasen, J. W.; Rouhanipour, A.; Breiby, D. W.; Pisula, W.; Müllen, K. The Influence of Morphology on High-Performance Polymer Field-Effect Transistors. *Adv. Mater.* **2009**, *21*, 209–212.
15. Zhang, W.; Smith, J.; Watkins, S. E.; Gysel, R.; McGehee, M.; Salleo, A.; Kirkpatrick, J.; Ashraf, S.; Anthopoulos, T.; Heeney, M.; et al. Indacenodithiophene Semiconducting Polymers for High-Performance, Air-Stable Transistors. *J. Am. Chem. Soc.* **2010**, *132*, 11437–11439.
16. Liu, X.; Guo, Y.; Ma, Y.; Chen, H.; Mao, Z.; Wang, H.; Yu, G.; Liu, Y. Flexible, Low-Voltage and High-Performance Polymer Thin-Film Transistors and Their Application in Photo/Thermal Detectors. *Adv. Mater.* **2014**, *26*, 3631–3636.
17. Wang, H.; Cheng, C.; Zhang, L.; Liu, H.; Zhao, Y.; Guo, Y.; Hu, W.; Yu, G.; Liu, Y. Inkjet Printing Short-Channel Polymer Transistors with High-Performance and Ultrahigh Photoresponsivity. *Adv. Mater.* **2014**, *26*, 4683–4689.
18. Li, W.; Hendriks, K. H.; Furlan, A.; Roelofs, W. S. C.; Wienk, M. M.; Janssen, R. A. J. Universal Correlation between Fibril Width and Quantum Efficiency in Diketopyrrolopyrrole-Based Polymer Solar Cells. *J. Am. Chem. Soc.* **2013**, *135*, 18942–18948.
19. Liang, Y.; Xu, Z.; Xia, J.; Tsai, S.-T.; Wu, Y.; Li, G.; Ray, C.; Yu, L. For the Bright Future—Bulk Heterojunction Polymer Solar Cells with Power Conversion Efficiency of 7.4%. *Adv. Mater.* **2010**, *22*, E135–E138.
20. Ha, J. S.; Kim, K. H.; Choi, D. H. 2,5-Bis(2-octyldodecyl)-pyrrolo[3,4-c]pyrrole-1,4-(2H,5H)-dione-Based Donor−Acceptor Alternating Copolymer Bearing 5,5′-Di(thiophen-2-yl)-2,2′-biselenophene Exhibiting 1.5 $cm^2 V^{-1} s^{-1}$ Hole Mobility in Thin-Film Transistors. *J. Am. Chem. Soc.* **2011**, *133*, 10364–10367.
21. Mei, J.; Kim, D. H.; Ayzner, A. L.; Toney, M. F.; Bao, Z. Siloxane-Terminated Solubilizing Side Chains: Bringing Conjugated Polymer Backbones Closer and Boosting Hole Mobilities in Thin-Film Transistors. *J. Am. Chem. Soc.* **2011**, *133*, 20130–20133.
22. Beaujuge, P. M.; Fréchet, J. M. J. Molecular Design and Ordering Effects in π-Functional Materials for Transistor and Solar Cell Applications. *J. Am. Chem. Soc.* **2011**, *133*, 20009–20029.
23. Gibson, G. L.; McCormick, T. M.; Seferos, D. S. Atomistic Band Gap Engineering in Donor-Acceptor Polymers. *J. Am. Chem. Soc.* **2012**, *134*, 539–547.
24. Tsao, H. N.; Cho, D. M.; Park, I.; Hansen, M. R.; Mavrinskiy, A.; Yoon, D. Y.; Graf, R.; Pisula, W.; Spiess, H. W.; Müllen, K. Ultrahigh Mobility in Polymer Field-Effect Transistors by Design. *J. Am. Chem. Soc.* **2011**, *133*, 2605–2612.
25. Zha, D.; Chen, L.; Wu, F.; Wang, H.; Chen, Y. Donor−Acceptor-Integrated Conjugated Polymers Based on Carbazole-[3,4-c:5,6-c]bis[1,2,5]thiadiazole with Tight $\pi-\pi$ Stacking for Photovoltaics. *J. Polym. Sci., Part A: Polym. Chem.* **2013**, *51*, 565–574.
26. Shin, J.; Um, H. A.; Lee, D. H.; Lee, T. W.; Cho, M. J.; Choi, D. H. High Mobility Isoindigo-Based π-Extended Conjugated Polymers Bearing Di(thienyl)ethylene in Thin-Film Transistors. *Polym. Chem.* **2013**, *4*, 5688–5695.
27. Bronstein, H.; Chen, Z.; Ashraf, R. S.; Zhang, W.; Du, J.; Durrant, J. R.; Tuladhar, P. S.; Song, K.; Watkins, S. E.; Geerts, Y.; et al. Thieno[3,2-b]thiophene-Diketopyrrolopyrrole-Containing Polymers for High-Performance Organic Field-Effect Transistors and Organic Photovoltaic Devices. *J. Am. Chem. Soc.* **2011**, *133*, 3272–3275.
28. Osaka, I.; Akita, M.; Koganezawa, T.; Takimiya, K. Quinacridone-Based Semiconducting Polymers: Implication of Electronic Structure and Orientational Order for Charge Transport Property. *Chem. Mater.* **2012**, *24*, 1235–1243.
29. Kang, I.; An, T. K.; Hong, J.-a.; Yun, H.-J.; Kim, R.; Chung, D. S.; Park, C. E.; Kim, Y.-H.; Kwon, S.-K. Effect of Selenophene in a DPP Copolymer Incorporating a Vinyl Group for High-Performance Organic Field-Effect Transistors. Effect of Selenophene in a DPP Copolymer Incorporating a Vinyl Group for High-Performance Organic Field-Effect Transistors. *Adv. Mater.* **2013**, *25*, 524–528.
30. Nielsen, C. B.; Turbiez, M.; McCulloch, I. Recent Advances in the Development of Semiconducting DPP-Containing Polymers for Transistor Applications. *Adv. Mater.* **2013**, *25*, 1859–1888.

31. Cho, M. J.; Shin, J.; Yoon, S. H.; Lee, T. W.; Kaur, M.; Choi, D. H. A High-Mobility Terselenophene and Diketopyrrolopyrrole Containing Copolymer in Solution-Processed Thin Film Transistors. *Chem. Commun.* **2013**, *49*, 7132–7134.
32. Kim, K. H.; Bae, S. Y.; Kim, Y. S.; Hur, J. A.; Hoang, M. H.; Lee, T. W.; Cho, M. J.; Kim, Y.; Kim, M.; Jin, J.-I.; et al. Highly Photosensitive J-Aggregated Single-Crystalline Organic Transistors. *Adv. Mater.* **2011**, *23*, 3095–3099.
33. Hoang, M. H.; Kim, Y.; Kim, M.; Kim, K. H.; Lee, T. W.; Nguyen, D. N.; Kim, S.-J.; Lee, K.; Lee, S. J.; Choi, D. H. Unusually High-Performing Organic Field-Effect Transistors Based on π-Extended Semiconducting Porphyrins. *Adv. Mater.* **2012**, *24*, 5363–5367.
34. Kim, J. H.; Lee, D. H.; Yang, D. S.; Heo, D. U.; Kim, K. H.; Shin, J.; Kim, H.-J.; Baek, K.-Y.; Lee, K.; Baik, H.; et al. Novel Polymer Nanowire Crystals of Diketopyrrolopyrrole-Based Copolymer with Excellent Charge Transport Properties. *Adv. Mater.* **2013**, *25*, 4102–4106.
35. Liu, Y.; Dong, H.; Jiang, S.; Zhao, G.; Shi, Q.; Tan, J.; Jiang, L.; Hu, W.; Zhan, X. High Performance Nanocrystals of a Donor–Acceptor Conjugated Polymer. *Chem. Mater.* **2013**, *25*, 2649–2655.
36. Lim, J. A.; Liu, F.; Ferdous, S.; Muthukumar, M.; Briseno, A. L. Polymer Semiconductor Crystals. *Mater. Today* **2010**, *13*, 14–24.
37. Li, H.; Wu, Y.; Wang, X.; Kong, Q.; Fu, H. A Self-Assembled Ultrathin Crystalline Polymer Film for High Performance Phototransistors. *Chem. Commun.* **2014**, *50*, 11000–11003.
38. Dong, H.; Jiang, S.; Jiang, L.; Liu, Y.; Li, H.; Hu, W.; Wang, E.; Yan, S.; Wei, Z.; Xu, W.; et al. Nanowire Crystals of a Rigid Rod Conjugated Polymer. *J. Am. Chem. Soc.* **2009**, *131*, 17315–17320.
39. Schwarz, K. N.; Kee, T. W.; Huang, D. M. Coarse-Grained Simulations of The Solution-Phase Self Assembly of Poly(3-hexylthiophene) Nanostructures. *Nanoscale* **2013**, *5*, 2017–2027.
40. Lee, S. G.; Kim, H.; Choi, H. H.; Bong, H.; Park, Y. D.; Lee, W. H.; Cho, K. Evaporation-Induced Self-Alignment and Transfer of Semiconductor Nanowires by Wrinkled Elastomeric Templates. *Adv. Mater.* **2013**, *25*, 2162–2166.
41. Li, Y.; Sonar, P.; Singh, S. P.; Soh, M. S.; van Meurs, M.; Tan, J. Annealing-Free High-Mobility Diketopyrrolopyrrole-Quaterthiophene Copolymer for Solution-Processed Organic Thin Film Transistors. *J. Am. Chem. Soc.* **2011**, *133*, 2198–2204.
42. Pokrop, R.; Verilhac, J.-M.; Gasior, A.; Wielgus, I.; Zagorska, M.; Travers, J.-P.; Pron, A. Effect of Molecular Weight on Electronic, Electrochemical and Spectroelectrochemical Properties of Poly(3,3″-dioctyl-2,2′:5′,2″-terthiophene). *J. Mater. Chem.* **2006**, *16*, 3099–3106.
43. Verilhac, J.-M.; LeBlevennec, G.; Djurado, D.; Rieutord, F.; Chouiki, M.; Travers, J.-P.; Pron, A. Effect of Macromolecular Parameters and Processing Conditions on Supramolecular Organisation, Morphology and Electrical Transport Properties in Thin Layers of Regioregular Poly(3-hexylthiophene). *Synth. Met.* **2006**, *156*, 815–823.
44. Tong, M.; Cho, S.; Rogers, J. T.; Schmidt, K.; Hsu, B. B. Y.; Moses, D.; Coffin, R. C.; Kramer, E. J.; Bazan, G. C.; Heeger, A. J. Higher Molecular Weight Leads to Improved Photoresponsivity, Charge Transport and Interfacial Ordering in a Narrow Bandgap Semiconducting Polymer. *Adv. Funct. Mater.* **2010**, *20*, 3959–3965.
45. Wang, S.; Wang, M.; Zhang, Xu.; Yang, X.; Huang, Q.; Qiao, X.; Zhang, H.; Wu, Q.; Xiong, Y.; Gao, J.; et al. Donor–Acceptor–Donor Type Organic Semiconductor Containing Quinoidal Benzo[1,2-b:4,5-b′]dithiophene for High Performance n-Channel Field-Effect Transistors. *Chem. Commun.* **2014**, *50*, 985–987.
46. Lei, T.; Guo, Z.-H.; Zheng, C.; Cao, Y.; Liang, D.; Pei, J. How Does a Supramolecular Polymeric Nanowire Form in Solution? *Chem. Sci.* **2012**, *3*, 1162–1168.
47. Kline, R. J.; McGehee, M. D.; Kadnikova, E. N.; Liu, J.; Fréchet, J. M. J.; Toney, M. F. Dependence of Regioregular Poly(3-hexylthiophene) Film Morphology and Field-Effect Mobility on Molecular Weight. *Macromolecules* **2005**, *38*, 3312–3319.
48. Zhou, Y.; Lei, T.; Wang; Pei, J.; Cao, Y.; Wang, J. High-Performance Organic Field-Effect Transistors from Organic Single-Crystal Microribbons Formed by a Solution Process. *Adv. Mater.* **2010**, *22*, 1484–1487.
49. Kalb, W. L.; Mathis, T.; Haas, S.; Stassen, A. F.; Batlogg, B. Organic Small Molecule Field-Effect Transistors with Cytop Gate Dielectric: Eliminating Gate Bias Stress Effects. *Appl. Phys. Lett.* **2007**, *90*, 092104.
50. Kalb, W. L.; Haas, S.; Krellner, C.; Mathis, T.; Batlogg, B. Trap Density of States in Small-Molecule Organic Semiconductors: A Quantitative Comparison of Thin-Film Transistors with Single Crystals. *Phys. Rev. B* **2010**, *81*, 155315.
51. Briseno, A. L.; Mannsfeld, S. C. B.; Ling, M. M.; Liu, S.; Tseng, R. J.; Reese, C.; Roberts, M. E.; Yang, Y.; Wudl, F.; Bao, Z. Patterning Organic Single-Crystal Transistor Arrays. *Nature* **2006**, *444*, 913–917.
52. Tang, Q.; Li, L.; Song, Y.; Liu, Y.; Li, H.; Xu, W.; Liu, Y.; Hu, W.; Zhu, D. Photoswitches and Phototransistors from Organic Single-Crystalline Sub-micro/nanometer Ribbons. *Adv. Mater.* **2007**, *19*, 2624–2628.
53. Cao, Y.; Wei, Z.; Liu, S.; Gan, L.; Guo, X.; Xu, W.; Steigerwald, M. L.; Liu, Z.; Zhu, D. High-Performance Langmuir–Blodgett Monolayer Transistors with High Responsivity. *Angew. Chem., Int. Ed.* **2010**, *49*, 6319–6323.
54. Cho, M. Y.; Kim, S. J.; Han, Y. D.; Park, D. H.; Kim, K. H.; Choi, D. H.; Joo, J. Highly Sensitive, Photocontrolled, Organic Thin-Film Transistors Using Soluble Star-shaped Conjugated Molecules. *Adv. Funct. Mater.* **2008**, *18*, 2905–2912.